Contents

1 Introduction

1.1 Mission description

This mission was organized in the framework of ESO contract N^o ODG/97-6276. Its aim was to perform the monitoring of the important optical turbulence parameter - the wavefront outer scale - with a new instrument, Grating Scale Monitor (GSM), developed at the Departement d'Astrophysique of the Nice University. The GSM campaign began on August 24 and ended on September 26, 1997. Initially foreseen at Paranal site, it has been shifted to La Silla. The reason is that, due to scheduled VLT integration, ESO was not in a position to offer acceptable working conditions for scientific experiments at Paranal summit before the UT1 "first light". Five persons participated in this mission :

F. MARTIN (Professor at Nice University, in charge of GSM experiment)
J. BORGNINO (Professor at Nice University)
A. TOKOVININ (Astronomer at Moscow University)
A. ZIAD (Maître de Conférences at Nice University)
R. AVILA (PhD student at Nice University)

The first 4 persons participated in the equipment deployment and tests (August 25-26) and assured the first half of the observing run (August 27 - September 6). Then, after a 3-day break, the measurements were resumed on September 10 with a partial change of the team (the last 3 persons on the above list remained). After the last night, September 19, the equipment was packed.

The weather statistics for the campaign is given in the table below. With these conditions, the 21 nights have produced a total of 115 hours of monitoring of the turbulence parameters (outer scale, Fried parameter and scintillation) distributed as indicated in Fig.1.

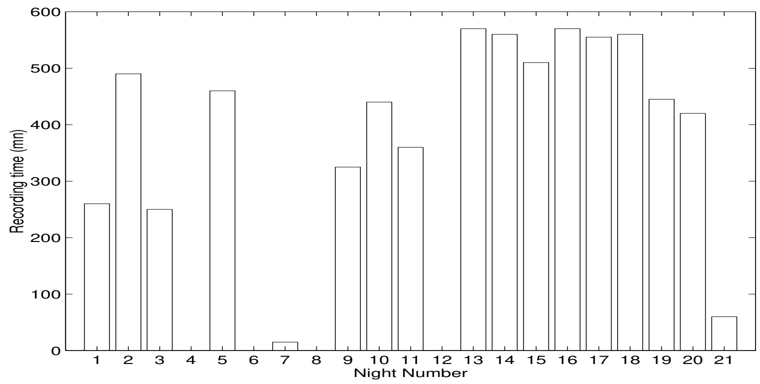

	First run	Second run	Total
Clear	4	6	10
Partial	3	3	6
Cloudy	4	1	5

Figure 1: The distribution of the total measuring time over the 21 nights of the campaign.

1.2 Instrument configuration

The GSM instrument consists of the following components:

- Four acquisition modules, each comprising the 10-cm Maksutov telescope, optical box, photomultiplier and associated electronics.
- Acquisition computer equipped with GSM interface board.
- Electronic box for signal distribution and power supply, together with cables.
- Three equatorial mounts "Astrophysics 900".

- Auxiliary material (second computer for backup and data processing, spare parts, instruments, etc.).

The on-site mission preparation consisted in building the 4 concrete piers. Also, a container-style building on the site was planned to serve as GSM office, but because of disastrous weather conditions before our arrival, it has been impossible for the ESO team at La Silla to accomplish this task. In spite of this, during the first day an important team of ESO (8 to 10 people), that we want to thank here, worked very hard to get the things ready in time; at the begining of the night all was finished and our equipment was put under cover in the GSM office, ready to work.

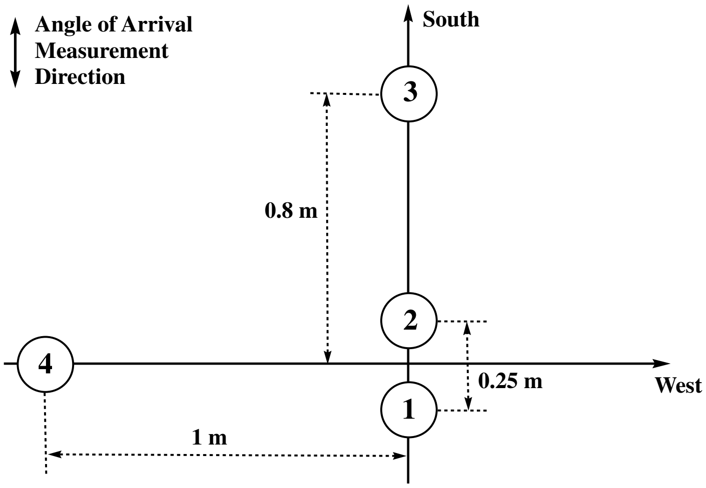

Figure 3: The GSM configuration.

GSM was installed on three piers. It was located near the ESO DIMM and ESO Schmidt telescope, on the pre-existing concrete platform (Fig. 2). The central pier held a mounting with two modules (1 and 2). At a distance of 0.8 m to the south the second pier with a mounting and module 3 was located. Third pier with module 4 was at 1.0 m to the east of the central one. Thus the instrument had a compact L-shaped configuration (Fig. 3). The distances between piers were chosen for optimal sensitivity of the angle of arrival (AA) covariance to outer scale. Telescope objectives were located 1.70 m above the ground level. A fourth pier, 1.2 m to the south of the pier 2, was also built to realize the linear configuration of GSM which served for experimental purposes.

The wind-induced telescope vibrations present a potential problem in AA measurements. To reduce their effect, the instrument was surrounded by a protective net (30 % wind transparency) from 3 sides (north, east and west). The net was 2 m high, and completely decoupled from piers.

The container-type building with computers and observers was located at a distance some 5 m from the central pier, to the south-west. With a prevailing wind from the North the GSM was supposed to be free from the locally generated turbulence, and the building was not troublesome either. On the other hand, with the southern wind GSM was in the turbulent lee created by its own building, by the Schmidt telescope dome and by the small rocks to the south. This effect was indeed detected by comparing the seeing measured by GSM with ESO DIMM on the nights of August 28-30.

1.3 Summary of the previous work

The development of the Grating Scale Monitor (GSM) experiment was started in 1991 at the Departement d'Astrophysique de l'Universite de Nice, as a continuation of the wavefront structure studies conducted by F.Martin, J.Borgnino and A.Ziad. A.Tokovinin from the Sternberg Astronomical Institute of the Moscow University participated in the GSM project from the beginning, as well as A.Agabi (initially a PhD student at Nice).

The first data were obtained in 1993 at the sites Mont Gros and Calern in the south of France. The instrument consisted then of a 20 cm Celestron telescope with a 2-channel angle of arrival (AA) detection module and 2 flat mirrors which defined the baseline. This version, called GSM1, is described by Martin et al. (1994), and the first measurements of $\mathcal{L}_0$ are published by Agabi et al. (1995). Additional information can be found in the thesis works of A.Agabi (1994) and A.Ziad (1993). GSM1 used Polar star as a light source.

The second stage of the GSM project, called GSM2, started in 1994 by the development of the individual detection modules coupled to 10 cm telescopes, with the aim to have 4 modules which work synchronously and in parallel. In order to be able to work in the southern hemisphere we had to use the equatorial mounts, which involved a long study of the guiding and vibration effects on the AA measurements. Ph. Bourlon who studied the vibrations of the 3.6 m ESO telescope has actively participated in the vibration investigations.

The interest that ESO has manifested in the development of GSM for the characterization of sites in Chili was supported, as a first step, by a loan of ESO mount for these experiments. As a second step, and in the framework of the contract No. 44030/VLT/95/6200/G.W.I. between ESO and Departement d'Astrophysique, the GSM2 software for 4-channel data acquisition was developed and a number of studies was conducted to validate the method of AA measurements and to estimate its performance. The final report on these studies (Martin et al., 1996), called hereafter REP1, gives the most consistent and up-to-date description of the GSM which passed from the experimental stage to the stage of a measurement instrument. The theoretical calculations needed for derivation of the outer scale from AA covariances are presented by Avila et al. (1997).

Realisation of GSM project would be impossible without financial support from the INSU (Institut National des Sciences de l'Univers) and M.E.N.R.T. (Ministère de l'Education Nationale, de la Recherche et de la Technologie). The support from ESO (European Southern Observatory) is gratefully acknowledged.

We wish to express our gratitude to the people of the Departement d'Astrophysique who helped to realize this project: A.Robini and B.Rossi for mechanical engineering, J-F.Manigault (†), A.Agabi and M.Azouit for electronics. The authors would like to thank also all the people of O.C.A. (Observatoire de la Cote d'Azur) who helped us to prepare the preliminary observing campaigns at Calern and Mont Gros sites. The help of the ESO staff at La Silla site is very much appreciated.

References

[1] Martin F., Tokovinin A., Agabi A., Borgnino J., Ziad A., 1994, Astron. Astrophys. Suppl. Ser., V. 108, p. 1.

[2] Agabi A., Borgnino J., Martin F., Tokovinin A., Ziad A., 1995, Astron. Astrophys. Suppl. Ser., V. 109, p. 557.

[3] Agabi A. , 1994, GSM: une expérience dédiée à la mesure des paramètres de cohérence des fronts d'onde en Haute Résolution Angulaire. Thesis, Nice University (in French).

[4] Ziad A., 1993, Estimation des échelles limites de cohérence spatiale des fronts d'onde et Optimisation des observations à Haute résolution Angulaire en Astronomie. Thesis, Nice University (in French).

[5] Martin F., Borgnino J., Ziad A., Agabi A., Avila R., Tokovinin A., 1996. Grating Scale Monitor (GSM). Un moniteur des paramétres de la turbulence intervenant en HRA tout particulirement dédiée la mesure de l'échelle externe de cohérence spatiale des fronts d'onde. (ESO Report) - REP1.

[6] Avila R., Ziad A., Martin F., Agabi A., Tokovinin A., 1997, Theoretic spatiotemporal analysis of angle of arrival induced by atmospheric turbulence as observed with the grating scale monitor experiment. J. Opt. Soc. Amer., V. A14, p. 3037.

2 Data acquisition and reduction

2.1 Observing procedure

A stellar source was selected from the list of five single bright stars (Table 2) that pass close to zenith at La Silla at this season. Due to the limitation of the possible hour angles (in the adopted configuration the telescopes could not be pointed at hour angle less than 1 h before meridian because they touched the piers) the selected star was usually some 40-30 min. before meridian at the start, and 2-4 h after meridian at the end of its observations (depending on the availability of a more suitable source). Thus, observations were obtained at zenith angles from 0^o to 45^o. At least once per night the modulation amplitude was checked and re-adjusted (its slight dependence on temperature was noted).

Table 1: Data on the stars used

Code	HR	R.A., Dec. (2000)						V	$B-V$	Spectral
		h	m	s	^{o}	$'$	$''$			type
aphe	99	0	26	17.0	-42	18	22	2.39	1.09	K0III
ssgr	7121	18	55	15.9	-26	17	48	2.02	-0.22	B2.5V
apav	7790	20	25	38.9	-56	44	6	1.94	-0.20	B2IV
agru	8425	22	8	14.0	-46	57	40	1.74	-0.13	B7IV
apsa	8728	22	57	39.1	-29	37	20	1.16	0.09	A3V

After pointing to the source, the telescopes were focused by looking at the modulation contrast and trying to maximize it. Then the acquisition sequence was started, interrupted every 30-40 minutes for re-centering of the star in the field of view. Signal was normally registered during 2 mn, and these acquisitions were repeated every 4 mn. Occasionally, longer or shorter acquisition times were used for exploratory purpose. Normal sequence of acquisitions was performed automatically, but it was commanded manually in special circumstances (clouds etc.). A manual observing journal was maintained as a supplement to computer database and as a place for various comments.

Immediately after acquisition the data were transferred to the second computer and processed. This enabled a quick acessment of data quality and results, including the seeing and $\mathcal{L}_0$. Processing time was about 30 s, and it would be possible to do processing and acquisition on the same computer at the adopted data rate. However, the availability of the second computer made data analysis easier and more flexible, and ensured a back-up.

2.2 Modifications of GSM software

General re-structuring of the existing software (as described in REP1) was done in the beginning of 1997 by A.Tokovinin. This permitted to distribute further software development between several persons. Thus, A.Ziad coded the baseline projection part (necessary for work on moving celestial sources) and the outer scale calculation (based on the interpolation of the pre-calculated normalized covariance grid). Further modifications were made at the site and mostly concerned the automatisation of data collection and processing. For example, a possibility was added to artificially degrade the temporal resolution during data reduction, in order to study the effects of integration time.

A new functionality of the GSM software is the storage of all parameters (except raw data) in a binary database file. For every acquisition the initial parameters (instrument configuration, star name, time) are stored. After data reduction the results are added to the same database. With more than a thousand data acquisitions performed during this mission, the database capability proved to be of vital importance for data management.

The very last modifications were made already after the completion of this mission and concerned the improved data reduction algorithm, as discussed in the next sub-section.

2.3 Data reduction algorithm

As explained in REP1, GSM data file consists of the 2-byte integer flux values recorded every 5 ms which correspond to the A, B, C, D signals in our notation. Thus, nominal data rate is 1600 bytes per second, and a standard 120 s acquisition occupies 192 KB of disk space. Relevant parameters and processing results are stored in the database file, hereafter called GSM.DAT. After every night the data were transferred to the back-up device for storage.

The data reduction can be decomposed into following three steps:

1. First pass: reading data file and computing modulation phase, contrast and flux. The corresponding formulae are given in Martin et al. (1994). The phases are computed as fractions of grating period and then an integer number of periods is added from phase continuity considerations. Sometimes, when noise spikes become comparable to the half-period, a phase jump may occur. Phase jumps are detected and eliminated during the first pass by a special filter (which, in fact, is the most time-consuming part at this stage). Filtered phases are stored as real numbers in a temporary file on a RAM disk, this file is erased after pass 2.

During first pass the mean flux, flux fluctuations, mean contrast and contrast fluctuations (as a mean square difference of adjacent contrast values) are computed as well. The computation of matrix elements for the rms parabolic trend adjustment is performed. The trend is caused by small residual linear motion due to imperfect orientation of mountings' axes.

2. Second pass (statistical calculations). The phases are read from temporary file. Trend is subtracted. Angle of arrival (AA) variances and covariances are computed. The photon and scintillation noise is subtracted from phase variances.

Noise estimate is based on the contrast fluctuations as computed during pass 1. It can be shown that the phase noise σ_p^2 (in units of grating period squared) is related to the contrast fluctuations σ_C^2 as follows:

$$\sigma_p^2 = \sigma_C^2 / [8\pi^2 C^2 (1 + 4C^2/\pi^2)], \tag{1}$$

where C is the mean contrast. This formula is obtained by calculating $< C^2 > - < C >^2$ under assumption that relative flux variations in the 4 channels ABCD are uncorrelated and are equal to δ. The relation between δ and σ_p^2 is given in REP1 and in Martin et al. (1994). For pure photon noise $\delta = 1/N$, N being the average number of photons per channel. Thus the *noise factor* $f_2 = \delta N$ is equal to 1 for poisson noise and is > 1 when scintillation noise is added.

Eq. (1) was verified by measuring photon noise in the laboratory. Also, the noise factor f_2 as calculated using this relation was compared to the direct f_2 measurements made on the nights of September 4/5, 5/6, 6/7 and 14/15, and a good agreement was found. Our previous experience has shown that scintillation noise is almost negligible (f_2 close to 1), but this was not the case for this mission, typical f_2 values being from 2 to 5. The difference is mostly explained by the fact that previous data were taken with a 20 ms time resolution and were much less sensitive to scintillation due to the specific time filtering in this regime. The scintillation at La Silla was rather strong because of the jet-stream generated high altitude turbulence.

The temporal averaging during 5 ms has negligible effect on the computed AA covariances and dispersions, but is non-negligible for differential AA variance σ_d^2 because its spectrum has more power at high temporal frequencies. A correction for time averaging is performed by computing additionally the AA variances with a degraded temporal resolution of 10 ms. Then the "true" variance corresponding to zero integration time is estimated as

$$\sigma_d^2(0\mathrm{ms}) = 2\sigma_d^2(5\mathrm{ms}) - \sigma_d^2(10\mathrm{ms}). \tag{2}$$

This linear extrapolation law was found from the study of exposure time influence conducted by A. Ziad and can be explained by the power-law character of the AA spectrum ($\sigma_d^2(\tau)$ continues to increase as τ approaches 0). In REP1 it was shown that the uncertainity of the correction for finite integration time constitutes a major source of measurement errors of σ_d^2. Now, when this correction is properly taken into account, this error term must not be included in the error calculation.

The scintillation index (flux variance normalized by the square of mean flux) is computed during pass 1 with a 5 ms time resolution from the variance of the sum of ABCD (thus annulating the flux modulation). It can also be corrected for temporal averaging in a similar manner, i.e. by comparing the 5 ms and 10 ms indexes and extrapolating linearly to 0 ms (this correction was *not* applied to the data presented below). It should be noted that a global flux variance for the whole acquisition is computed, and it is sensitive to the low-frequency flux variations, e.g. due to clouds. The scintillation index for partially cloudy nights is thus overestimated and must not be used for high altitude turbulence characterization.

3. Third pass. The AA covariances normalized by the differential variance are compared to the theoretical normalized covariances which are stored in a file for a grid of baseline coordinates (x, y) and a logarithmic grid of outer scale values. For each baseline its projection onto the sky is calculated, using the time of acquisition (to compute the hour angle), the star name code (to look for its coordinates) and the site code (to look for site coordinates). Then the theoretical covariances as a function of $\mathcal{L}_0$ are found by interpolating the grid to the projected baseline. Finally the appropriate $\mathcal{L}_0$ for each baseline is determined. The adopted value of the outer scale is taken as a median of the 6 individual values corresponding to each baseline. When a measured covariance did not provide an outer scale, e.g. being too large, this baseline was not taken into account in median calculation. The error of the final $\mathcal{L}_0$ values is computed from the scatter of the 6 individual estimates. We checked that the errors on $\mathcal{L}_0$ computed from noise considerations as detailed in REP1 are similar to the "statistical" errors obtained from the scatter.

At the third pass the r_0 values calculated from the AA dispersion of each module are corrected for the outer scale, to compare them to the "differential" r_0. This enables to estimate the importance of telescope vibrations.

It must be noted that small variations of the measured normalized covariances lead sometimes to significant changes of the derived $\mathcal{L}_0$, because theoretical curves corresponding to different $\mathcal{L}_0$ are rather close to each other. Thus, the corrections of the scintillation noise and of the effect of finite integration time were important, because they changed the σ_d^2 by some 10–20%. For example, it was found that with the integration time of 10 ms the derived $\mathcal{L}_0$ are systematically higher than the "true" $\mathcal{L}_0$ as given by the procedure described above.

2.4 Various tests concerning data quality

A certain effort has been devoted to ensure that the AA fluctuations measured by GSM modules are free of instrumental effects. Most troublesome of these are the mechanical errors caused by the telescopes.

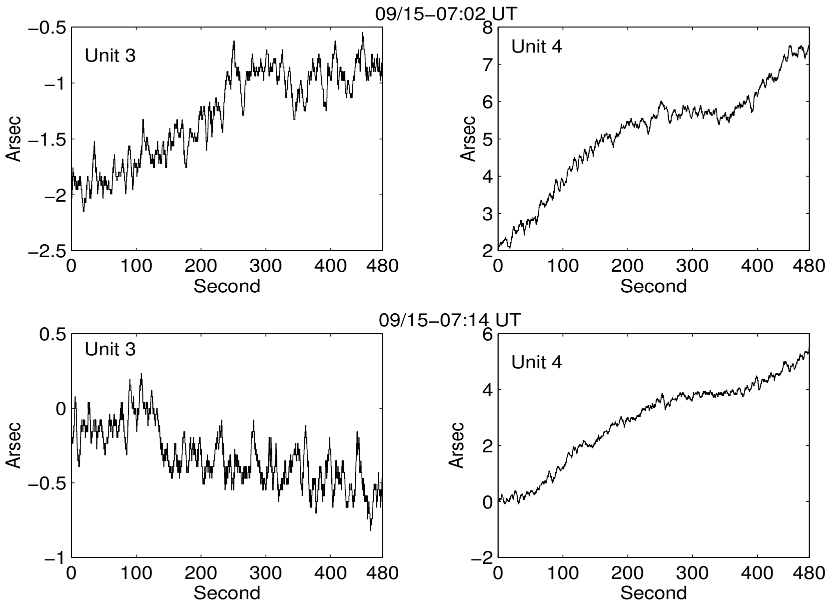

Figure 4: The two 8 mn low-pass filtered recordings of AA on modules 3 and 4 showing the low-frequency component due to hour drive (note the different vertical scales). For standard 2 mn acquisitions this component is effectively removed by parabolic trend fitting.

2.4.1. Telescope guiding errors. The AA fluctuations are measured in the declination direction and hence must not be directly sensitive to guiding errors. However, some residual low-fequency component due to the hour drive was still present in the signal of modules 3 and 4 (but not 1 and 2), as shown in the figure. The period of the hour drive worm is 4 minutes, and in the 2 min standard acquisitions a low-frequency component resembles the half-period of the sinusoid (Fig. 4). It arises presumably because of the mechanical coupling of telescope motions in hour angle and declination, due to the imperfect worm gear adjustment. Fortunately, the amplitude of this component is small ($< 0.5''$) and most of it is removed when a parabolic trend is subtracted. We checked that a subtraction of higher-order polynomial trend does not change the results.

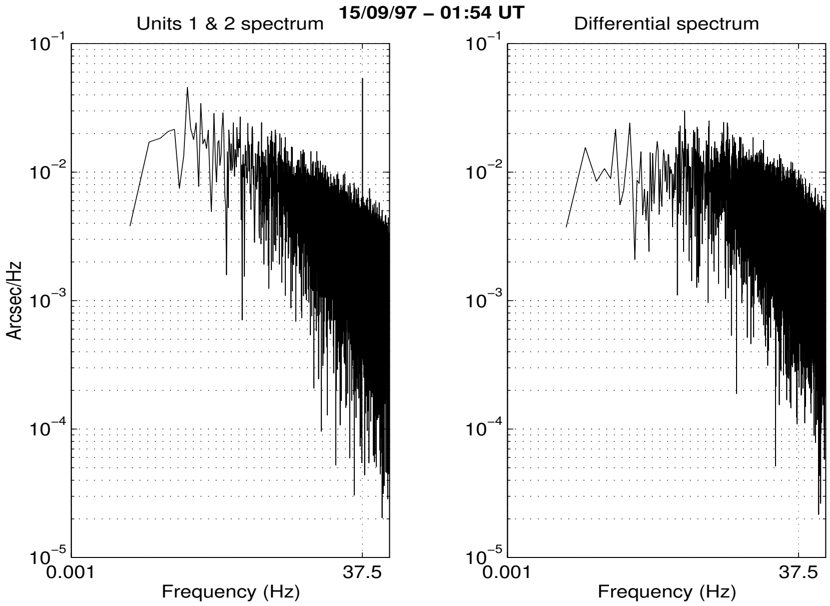

Figure 5: The power spectrum of AA fluctuations in module 1 and of the difference between the signals of modules 1 and 2 (log-log scale). The 37.5 Hz vibration in both signals is due to hour drive stepping motor, it is annulated in the differential signal.

2.4.2. Telescope high-frequency vibrations are caused by the stepping motor of the hour drive and produce a fundamental frequency of 37.5 Hz (its higher and lower harmonics are also seen in the signal of module 3). The existence of this vibration was evident already during the laboratory tests of the mounts (made with the participation of Ph. Bourlon who measured vibrations by sensitive accelerometric equipment). This component is seen in the power spectra of AA (Fig. 5). However, the total power of vibrations is negligible as compared to the AA fluctuations power, and vibrations were not taken into account in the standard signal processing described above. For some critical applications like the study of temporal cross-correlation functions the periodic vibrations were removed by signal filtering in the frequency domain.

2.4.3. Telescope vibrations caused by the wind are controlled by comparison of the r_0 as calculated from AA variance (vibration-sensitive) to the differential r_0 (vibration-insensitive). Even for wind speed of 15 m/s no effect can be seen in the definitively reduced data (Fig. 6). (The systematic difference existed in the initial data reductions because differential measurements were not corrected for 5 ms integration time averaging).

We believe that even at strong wind the vibrations remain uncorrelated and do not influence the measured AA covariances. This is because the telescopes were installed on separate mounts and piers. To verify this assumption, on the nights of September 4/5, 15/16, 16/17, 17/18 we removed temporarily the wind-protection nets and found that the results obtained were not different from those with nets, although the telescope vibrations without nets must be stronger (the net reduces wind speed at the telescopes by roughly a factor of 0.3). It can not be excluded, however, that wind gusts caused some correlated low-frequency component in the AA measured by all 4 modules, thus overestimating the covariances. The nights of September 14/15 and 18/19 with the largest measured outer scale were also the nights with the strongest wind.

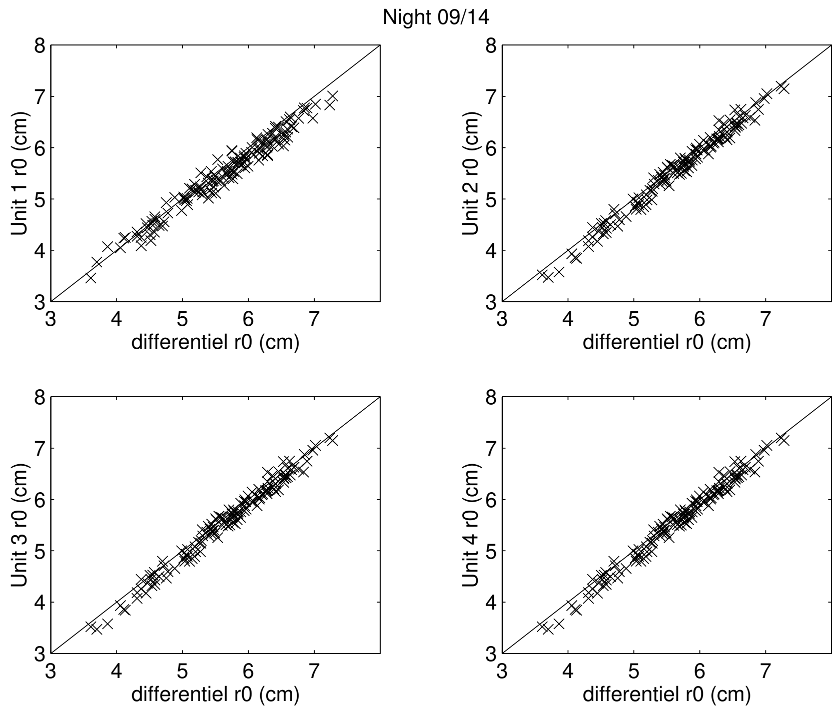

Figure 6: Comparison of the r_0 estimated from the AA variance and corrected for the finite $\mathcal{L}_0$ with the r_0 from differential AA variance. On the night of September 14/15 with a 15 m/s wind the wind-induced telescope vibrations are still not apparent.

2.5 Auxiliary data

The data from the sources other than GSM are given in this report in order to have a better idea on the meteorological conditions during our mission. The ESO meteorological service provided the main parameters of the weather at the site with a 20 mn temporal resolution, namely ground wind speed and direction, temperature and relative humidity.

A wind speed in the upper atmosphere over La Silla (at 200 mb level) was deduced from the atmospheric model charts consulted at the WEB site *http://grads.iges.org/pix/sa.fest.html*. In a similar way, the satellite images of South America (accessed through the La Silla WEB site) provided the overview of the global weather pattern.

The data on La Silla seeing measured by ESO DIMM are available for comparison with our measurements, as discussed below. In particular, this comparison helped to estimate the contribution of the lowermost ground layers, because the height of the two instruments was different.

Independent measurements of $\mathcal{L}_0$ and seeing were obtained with the ADONIS adaptive optics system on the ESO 3.6 m telescope during 1 hour on the night of August 29/30. A good general agreement with GSM was noted. We discuss this data set in the Appendix.

3 Mission results

3.1 Data file description

All individual measurements of seeing, outer scale and scintillation are given in electronic form as an ASCII text file *gsm97*. Its columns contain the following data:

- Date (mm.dd)
- Universal time (hh.mm) corresponding to start of acquisition
- Configuration (*St.* for standard, *L.* for linear)
- Asquisition time (s)
- Star code (see Table 1)
- Zenith distance (degrees)
- Flux per ABCD per acquisition (counts), corresponding roughly to the flux in 10^3 counts$\cdot s^{-1}$.
- FWHM seeing angle (arcseconds) at 500 nm wavelength as deduced from differential AA variance (FWHM $= 0.98\lambda/r_0$).
- $\mathcal{L}_0$ (m)
- scintillation index σ_I^2 (%) with 5 ms integration time, corrected for zenith distance dependence (multiplication by $(\cos z)^{8/3}$).

3.2 General data overview

The summary of the measurement results for each night is given in the Table 2. Corresponding meteorological data are given in the Table 3.

Each night is identified by its sequential number and date. The night of August 26/27 was devoted to the instrument installation, so it was assigned number 0. For the sake of completeness we retain in Tables 2 and 3 this night and other 2 nights with small (< 10) number of measurements (these dates are marked by asterisks in the Tables). The nights number 4,6,8 were completely cloudy and are not represented in the Tables, thus leaving the 16 nights with useful data.

In the first columns of Table 2 we give night number, date, universal time of measurements start and end, total number of measurements N. The following three pairs of columns contain data on seeing (FWHM angle at 500 nm), wavefront outer scale $\mathcal{L}_0$ and scintillation index σ_I^2. For each of these parameters the median value for the night is given in the first column, and the range of its variation (the values that correspond to the 10% and 90% percentile levels of nightly cumulative distributions) is given in the second column. It must be again noted that scintillation index values are not corrected to zenith and are measured with 5 ms time resolution; they can be overestimated for partially clear nights because of transparency variations.

Table 2: The summary of GSM results for each night

No.	Date 1997	UT, hh.mm Start	End	N	Seeing, arcsec Med.	Range	$\mathcal{L}_0$, m Med.	Range	Scintillation, % Med.	Range
0	26/27*	4.24	7.32	7	0.57	0.51–0.89	13.4	9.1 –21.0	0.6	0.0–1.2
1	27/28	2.09	8.43	53	0.97	0.76–1.22	14.4	2.9 –27.1	3.4	2.1–5.1
2	28/29	23.30	8.48	127	1.62	0.96–2.01	14.1	7.9 –22.3	3.6	2.2–6.9
3	29/30	0.21	5.36	75	1.03	0.62–2.03	19.5	9.8 –38.7	1.4	0.8–2.3
5	31/01	0.54	9.25	81	1.62	1.04–2.10	27.3	16.5–71.8	7.7	2.2–23.1
7	02/03*	0.09	0.32	7	1.54	1.41–1.76	23.6	25.8–96.4	6.2	5.4–72.0
9	04/05	0.53	9.49	68	1.58	1.24–1.91	24.5	15.3–33.6	4.4	2.1–11.9
10	05/06	23.55	9.11	113	1.59	1.24–1.95	29.7	35.2–54.8	4.0	2.0–6.1
11	06/07	23.43	6.00	88	1.48	1.25–1.85	23.7	15.3–44.3	3.0	1.9–8.1
12	10/11*	0.49	1.37	5	1.32	1.25–1.43	17.4	20.2–32.7	4.6	2.8–10.8
13	11/12	23.38	9.04	111	2.06	1.67–2.72	16.6	11.2–24.6	4.6	3.2–7.1
14	12/13	23.55	9.13	134	1.79	1.35–2.44	23.3	13.8–41.5	7.3	4.7–11.2
15	13/14	0.58	9.28	115	2.07	1.46–2.69	27.9	17.1–41.3	4.6	3.4–5.9
16	14/15	23.44	9.19	138	1.78	1.53–2.28	35.6	18.5–57.8	3.5	2.1–6.9
17	15/16	23.47	8.59	116	1.22	0.87–1.82	18.7	10.6–34.5	3.1	2.0–5.8
18	16/17	23.52	9.10	130	1.71	1.41–2.21	27.7	12.1–57.2	3.9	2.4–5.7
19	17/18	23.46	7.03	47	1.44	1.10–2.09	23.1	11.6–36.9	3.5	2.2–6.6
20	18/19	1.38	8.28	79	2.43	1.88–3.08	45.9	28.0–111.8	5.0	2.9–7.3
21	19/20	0.03	1.04	13	1.07	0.98–1.14	20.9	13.5–43.4	2.5	1.7–4.8

Table 3: The summary of meteo data

No.	Date 1997, 08-09	Wind Speed, m/s	Range, m/s	Dir., deg.	Tempe- , rature, ^{o}C	Rel. hum., %	Wind at 200 mb, m/s	Clouds
0	26/27*	1.1	0.2–2.6	175.8	17.7	20	-	Clear
1	27/28	1.6	0.2–4.4	172.8	18.2	16	25	Clear
2	28/29	2.9	0.4–7.1	174.0	16.4	26	-	Clear
3	29/30	2.4	0.6–6.4	172.0	14.1	42	35	Partial
5	31/01	7.2	4.0–15.0	32.5	11.1	42	35	Partial
7	02/03*	11.8	8.1–16.0	31.2	10.1	25	60	Cloudy
9	04/05	8.0	3.6–11.4	46.0	12.1	28	40	Partial
10	05/06	13.8	10.–16.8	22.5	9.8	44	-	Clear
11	06/07	9.6	7.2–11.0	22.5	8.8	39	-	Clear
12	10/11*	8.4	6.9–10.0	25.5	12.5	15	70	Cloudy
13	11/12	10.6	7.1–12.2	23.0	7.9	20	60	Partial
14	12/13	8.5	6.8–10.4	18.5	6.9	35	75	Clear
15	13/14	6.6	1.6–11.8	19.0	7.4	40	70	Clear
16	14/15	14.8	9.1–17.4	108.3	13.9	15	-	Clear
17	15/16	3.7	2.2–6.6	48.5	14.0	19	45	Clear
18	16/17	8.0	5.2–12.6	189.5	15.6	23	-	Clear
19	17/18	9.8	1.8–16.8	47.0	17.3	30	50	Partial
20	18/19	13.2	8.9–20.2	115.0	7.8	82	55	Clear
21	19/20	7.0	6.2–7.6	33.0	10.4	64	45	Partial

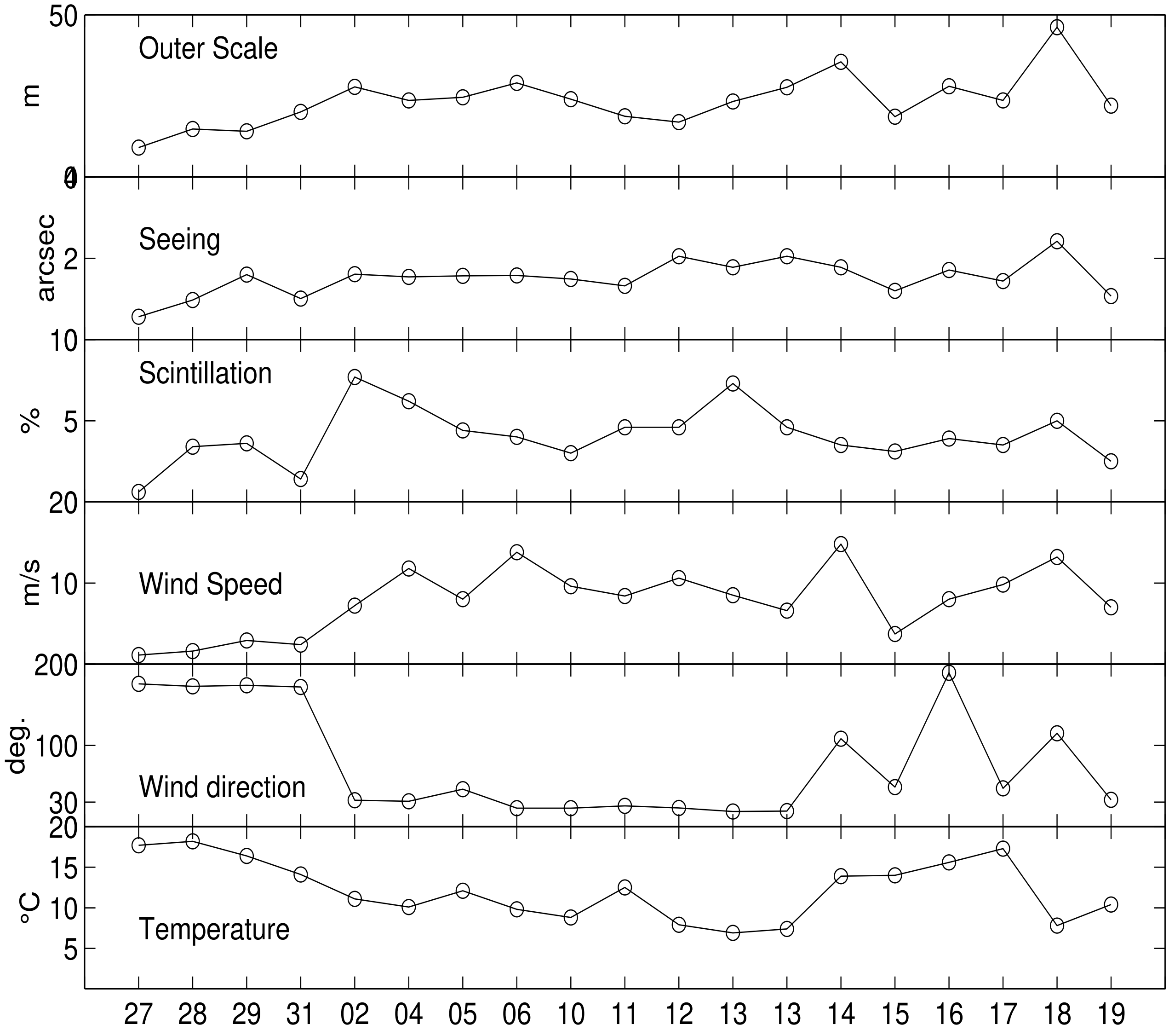

Figure 7: Evolution of nightly median values of seeing, outer scale, scintillation, wind speed, wind direction and temperature during the mission.

Table 3 consists of 3 parts. The first 2 columns repeat the night number and date. Next 3 columns contain information on ground wind: median speed, range (from min to max) and median direction. In the last 4 columns median values of temperature and relative humidity are given, as well as the rough estimate of wind speed at 200 mb level (not for every night) and cloud coverage.

The figures 7, 8, 9 give a general representation of the seeing, outer scale, and meteo data evolution during the mission. The whole 21 nights can be sub-divided into three periods according to the atmospheric conditions:

First period from August 26 to August 29 was characterized by slow southern wind and reasonably good seeing. The best seeing ($0.5''$) was registered during the instrument tests on the night of August 26/27. During each night important seeing variations ($> 0.5''$) were observed, presumably because of changing ground layer contribution.

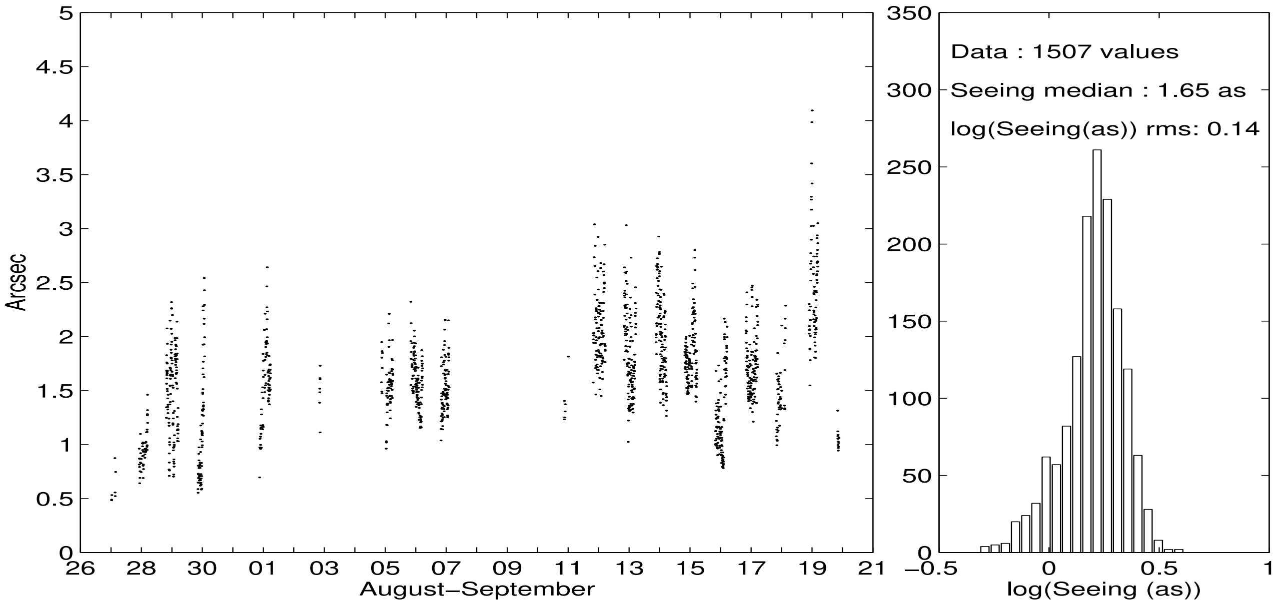

Figure 8: All measurements of seeing for this mission are plotted against time. Right pannel shows the histogram of log(seeing).

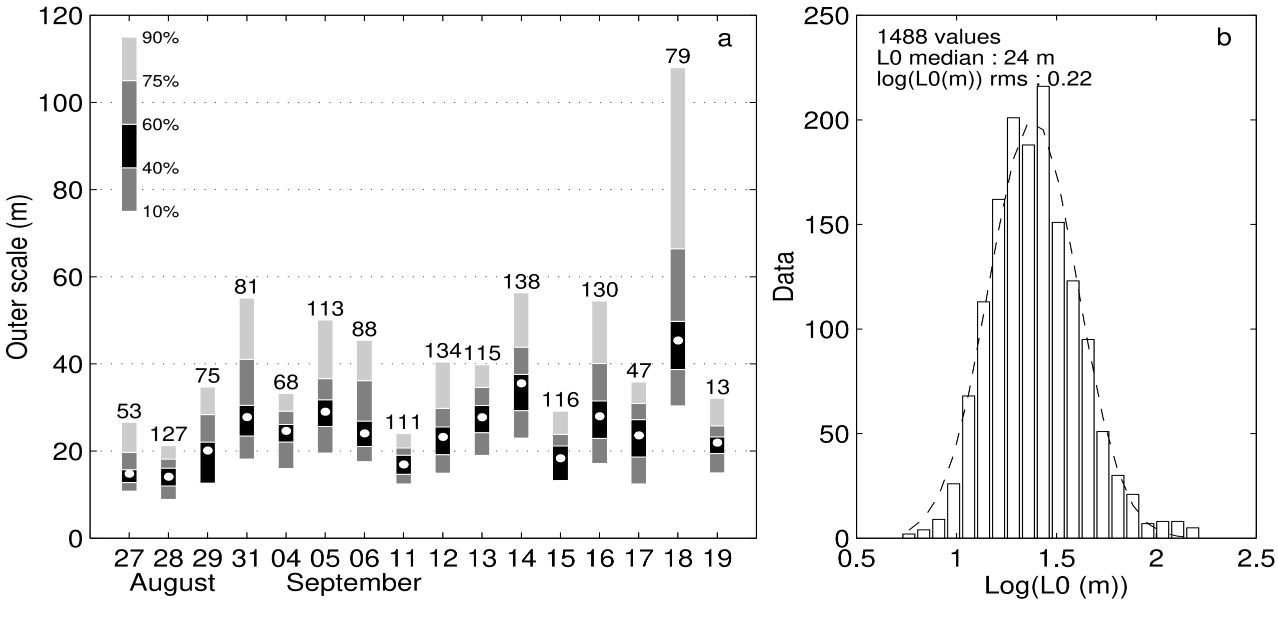

Figure 9: The distribution of outer scale values for each night is represented by grey-scale bars which depict selected levels of the cumulative histogram. Median values are plotted as circles. On the right the histogram of $\log\mathcal{L}_0$ is shown, with a fitted log-normal distribution plotted in dashed line.

Second period from September 2 to September 13 was marked by a jet stream activity over La Silla (wind speed at 200 mb reaching 75 m/s). Stable ground wind around 10 m/s from north was persistent, and locally generated turbulence was "gone with the wind". The seeing and $\mathcal{L}_0$ were very stable, with only small variations from night to night. Scintillation was higher than in the first period. The 3-day break was in the middle of this period, and we might expect that during these days the conditions did not change either.

Third period from September 14 to September 19 was characterized by significant variations of all meteo parameters from night to night. Unfortunately, the seeing remained very bad, with only slight improvement on September 15 and exceptionally bad seeing on September 18. On the nights of September 14 and 18 there was a strong eastern wind of 15 m/s, and median $\mathcal{L}_0$ values for these nights were also the largest for this mission.

The median seeing registered during this campaign ($1.65''$) was much worse than typical seeing for this season (around $1''$), while the percentage of clear and semi-clear nights (2/3) was close to statistical expectations.

3.3 The wavefront outer scale statistics

The evolution of the nightly median values of $\mathcal{L}_0$ and few characteristic levels of nightly cumulative distributions are represented in Fig. 9. The variations from night to night are apparent. There is some correlation of nightly median $\mathcal{L}_0$ with seeing (the best seeing of August 27/28 corresponds to small $\mathcal{L}_0$, and the night of September 18/19 gave the worst seeing and the largest $\mathcal{L}_0$) and the average wind velocity.

The distribution of $\log\mathcal{L}_0$ for the whole mission is remarkably well represented by a log-normal law (corresponding significance level $P(\chi^2) = 0.24$), see Fig. 9. Median value of $\mathcal{L}_0$ is 24 m, rms scatter of $\log\mathcal{L}_0$ is ± 0.22, or ± 1.67 times from the median. The distributions of $\mathcal{L}_0$ for individual nights also resemble log-normal curves, with a larger scatter.

Continuous monitoring of $\mathcal{L}_0$ permitted for the first time to investigate the temporal evolution of this atmospheric parameter. Examining the curves of $\mathcal{L}_0$ (t) for individual nights, one finds two typical phenomena:

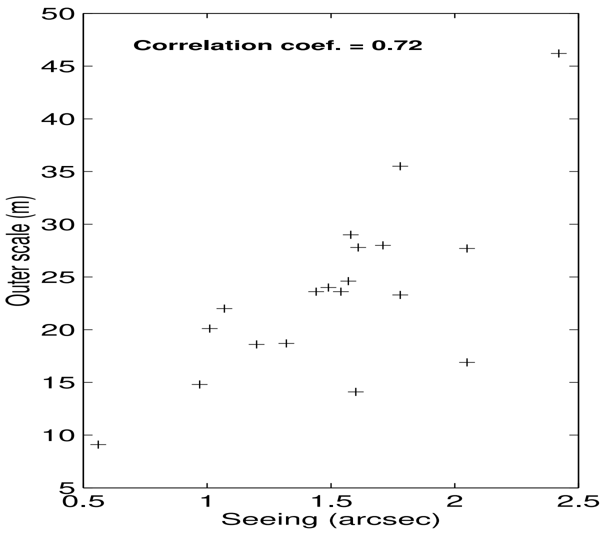

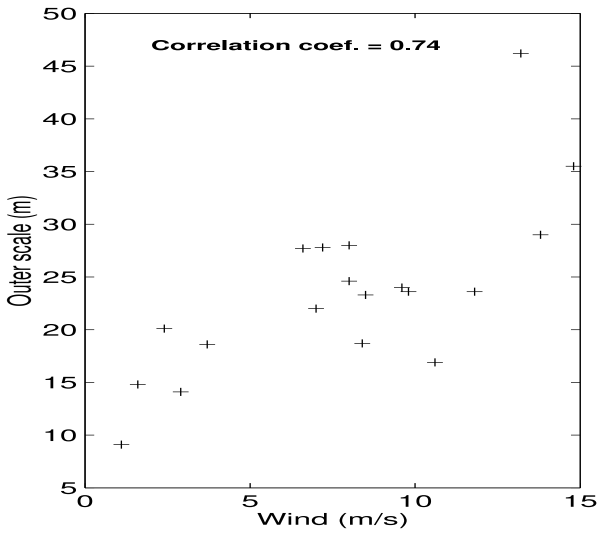

Figure 10: The correlation of median $\mathcal{L}_0$ for each night with the median nightly values of seeing and ground wind speed.

- There are periods of higher-than-average outer scale values of approximately 1 hour duration, e.g. the maxima around 2-3h UT observed on the nights of September 06/07, 15/16, 16/17, 18/19.
- The isolated high $\mathcal{L}_0$ values ("bursts") are found, e.g. at 6h10m UT on August 28/29. They are present not on all nights and are not very numerous. These bursts were noted already during the mission, but subsequent data reduction has proved that sometimes apparent bursts corresponded to the short periods of fast seeing, with attendant reduction of the measured differential variance and thus the increased normalized covariances. After the proper correction for exposure time effects the number of bursts was reduced, and overall values of derived $\mathcal{L}_0$ became smaller. However we believe that the remaining bursts correspond to the genuine increase of low-frequency wavefront corrugations. The similar $\mathcal{L}_0$ bursts were noted in ADONIS measurements. We looked for a change of the modulus of temporal cross-spectra of AA fluctuations during the burst and just after or before it, and have not found any significant difference.

The correlation between $\mathcal{L}_0$ and seeing exists for some nights (e.g. the nights of August 31/01, September 06/07, 13/14, 17/18) and is absent or not significant for other nights. However, the correlation between nightly median values of $\mathcal{L}_0$ and seeing seems to hold (Fig. 10), with a correlation coefficient of 0.72.

If we try to compare the temporal behaviour of $\mathcal{L}_0$ with the variations of seeing, scintillation and wind, no clear picture emerges: sometimes the seeing and $\mathcal{L}_0$ increase together (e.g. on September 06/07 at 6h UT), but more frequently the variations of these parameters seem to be independent (e.g. on September 05/06 when the significant $\mathcal{L}_0$ variation occured under constant seeing and constant ground wind conditions).

3.4 Comparison GSM - ESO DIMM

During our mission the two site-testing instruments, GSM and ESO DIMM, were installed near each other and worked simultaneously, which gives a unique opportunity to compare their results. ESO DIMM data on seeing were taken from the ESO meteo server and compared to GSM directly after time adjustment (for GSM, the moments of measurement start are given, while DIMM moments correspond to the end of integration). As shown in Fig. 11, the seeing measured by the two instruments shows remarkably similar temporal evolution. A good agreement between the GSM and DIMM seeing values exists for some moments or periods of time only, otherwise GSM measures the seeing which is always *not less* than the DIMM seeing.

The evident reason for this systematic difference is that the instruments were installed at a different height above ground (1.7 m for GSM and 5 m for DIMM). Thus, GSM seeing is contaminated by the additional contribution of the 3.3m-thick ground layer with strong turbulence. This contribution was particularly important on the nights of August 27-29 with a slow southern wind. In these conditions GSM was affected by a turbulent lee from its container, Schmidt telescope dome and small rocks to the south. It is noteworthy that during the periods of the best seeing on these nights both instruments agreed perfectly, which validates the explication given above.

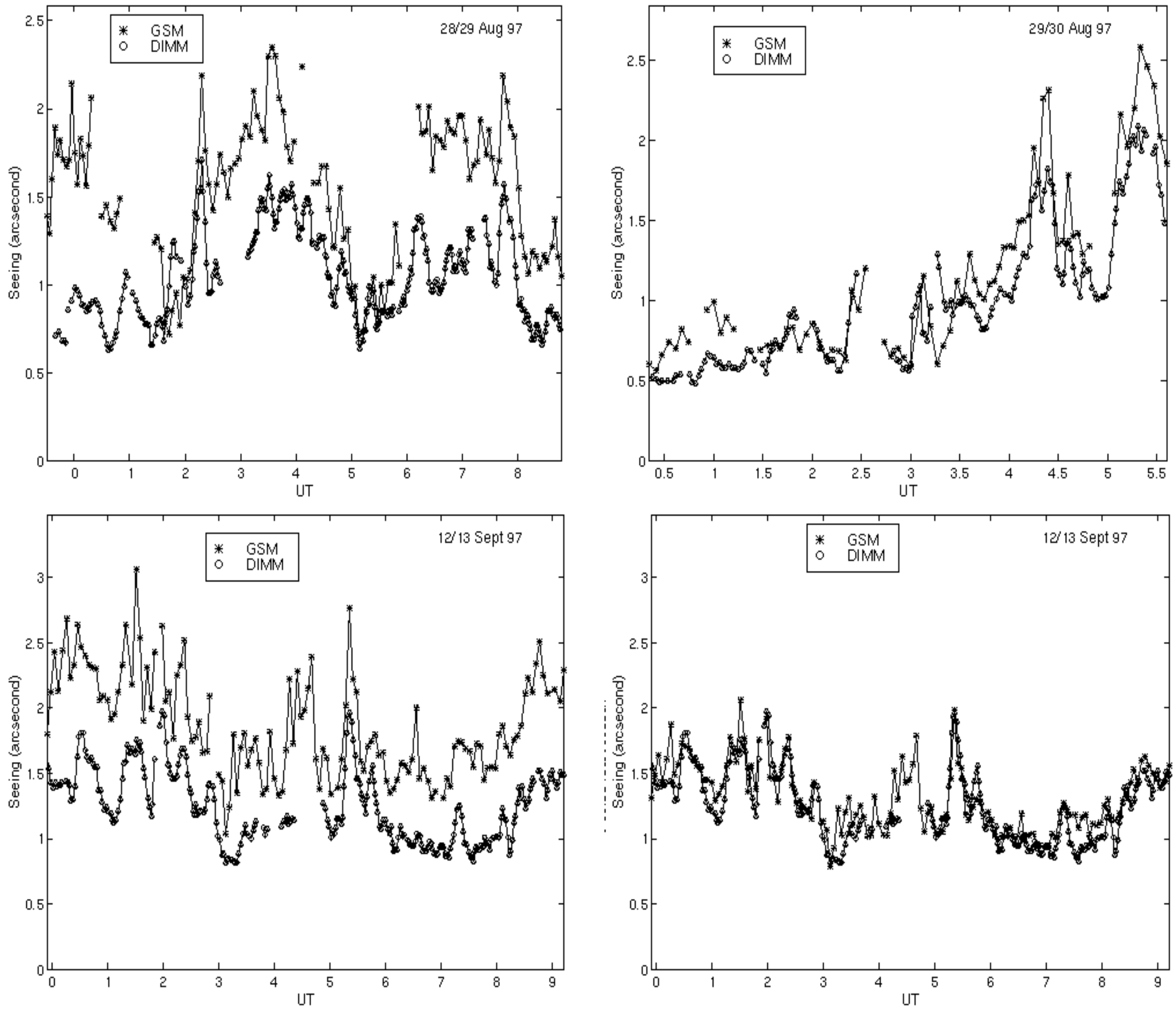

Figure 11: The comparison of seeing as measured by GSM and ESO DIMM for three nights. Ground turbulence influence is visible on the night of August 28/29, and less important on the night of August 29/30. On September 12/13 (lower left pannel) the systematic difference is due to the 10 ms time averaging of DIMM: when the GSM data are processed with 10 ms time resolution, a good agreement with DIMM is found (lower right pannel).

It must be noted that while DIMM is less sensitive to ground layer turbulence, it is by no means completely free of its influence. Indeed, the large seeing variations found on the night of August 28/29 by GSM are also followed by DIMM, but with a reduced amplitude. The height of 5 m above the ground is not sufficient to get rid of ground turbulence under slow wind conditions.

Yet another reason for the discrepancy between GSM and DIMM lies in their exposure time difference (10 ms for DIMM and 0 ms extrapolation for GSM). The temporal spectrum of the differential AA variance contains energy at high frequencies which is not sampled with the available time resolution, especially under fast seeing conditions encountered during the second and third periods of our mission. On these nights the ground turbulence was swept away by the strong wind, and seeing was very stable. Systematic constant difference between GSM and DIMM at the 10-20 % level was noted. This difference disappeared when GSM data were processed with the decreased time resolution of 10 ms (Fig. 11).

The combination of the two effects fully explains the systematic difference between GSM and DIMM seeing data. A perfect agreement between these instruments on the periods when these effects were not significant proves that their independent calibrations are correct and that reliable results on seeing can be obtained with both instruments.

The additional validation of GSM seeing measurements comes from the comparison with simultaneous data obtained with ADONIS on August 29/30, and from the comparison with estimates of NTT seeing made occasionaly from image width during our campaign.

3.5 Temporal behaviour of wavefront

The temporal cross-correlation functions of AA fluctuations on all 6 GSM baselines were calculated by R.Conan. The displacement of their maxima can be used to derive the effective wavefront speed (both velocity and direction), as shown by the example given in the Appendix (A&A Letter). The temporal analysis of the total data of this mission is not yet completed.

3.6 Comparison with ADONIS

On the night of August 29/30 $\mathcal{L}_0$ and seeing were measured by M.Sarazin and J.-L.Beuzit with the adaptive optics system ADONIS on the 3.6 m ESO telescope. A good general agreement with simultaneous GSM data was found, although there was no detailed correlation between the individual measurements (the instruments were separated by more than 1 km). More details on this experiment can be found in the Appendix (SPIE paper).

4 Conclusions and perspectives

The GSM campaign at La Silla has led to the following main results:

- The average value of the wavefront outer scale $\mathcal{L}_0$ during our mission was 24 m.
- The distribution of $\mathcal{L}_0$ is well approximated by a log-normal one, with a standard deviation of ± 1.67 times from the median.
- Temporal evolution of $\mathcal{L}_0$ was explored for the first time. It changes with a timescale of about 1 hour, with rare isolated high values ("bursts").
- A positive correlation between $\mathcal{L}_0$ and seeing exists for some nights, as well as for the nightly median values which are also correlated with median wind speed.
- Comparison between GSM and ESO DIMM shows a good calibration agreement between these instruments, and demonstrates the important effects of ground turbulence and of exposure time in seeing measurements.

The data obtained during this mission will be further processed to extract the effective wavefront velocity (and calculate adaptive optics time constant) and isoplanatic angles. Taken together, these results will lead to almost complete characterization of the site for high angular resolution imaging techniques like interferometry and adaptive optics. GSM is thus evolving towards a "Generalized Seeing Monitor".

Future missions are planned to explore other potentially interesting or important sites: ESO Paranal site in Chili, Cerro Pachon Gemini site in Chili, Oukaïmeden site in Maroc, Maidanak site in Uzbekistan, and others. Comparison of relevant atmospheric parameters of these sites will provide a solid basis for the performance analysis of the existing and planned high-resolution astronomical instruments, and will serve as a guideline for future instrument location choice.

5 Night-by-night data

The next 16 pages of this report contain the graphic representation of atmospheric turbulence and meteo parameters for each of the 16 clear or partially clear nights. For convenience, the mean nightly parameters from Tables 2 and 3 are repeated. Small comments are also given on meteo conditions or non-standard instrument configurations.

On each page, the upper left graph represents the $\mathcal{L}_0$, scintillation index (zenith-corrected, 5 ms integration time) and seeing plot in a semi-log scale. Short gaps in the data correspond usually to a change of star, while larger gaps are caused by clouds on partially clear nights. Temporal evolution of $\mathcal{L}_0$ can be better viewed on the middle left plot where it is represented in linear scale with "$\pm\sigma$" error bars (note that the scale was adjusted for better representation, and few high values of $\mathcal{L}_0$ are not plotted, e.g. on August 29/30). Upper right plot shows $\mathcal{L}_0$ - seeing correlation (with two regression lines), the middle right plot is a histogram of $\log\mathcal{L}_0$ for the night. The 3 lower plots depict the main meteo parameters evolution during each night.